Nonlinear Dyn (2025) 113:34191–34204
https://doi.org/10.1007/s11071-025-11787-9

RESEARCH

Noise-Assisted Synchronization in Networks of Coupled Mathieu-Duffing Oscillators

Thomas Breunung · Balakumar Balachandran

Received: 10 February 2025 / Revised: 5 August 2025 / Accepted: 3 September 2025 / Published online: 9 September 2025

Abstract Studies of collective behavior of coupled dynamical entities continue to reveal a broad range of phenomena, including synchronization. This behavior has often been analyzed by using models such as the Kuramoto model. The dynamics of this model has been related to dynamics of a diverse range of systems, for example, Josephson junctions, laser systems, power grids, and even, systems in sociology. With mechanical systems, synchronization has been commonly analyzed in systems, which exhibit limit cycle oscillations. Utilizing limit cycle oscillations allows one to draw analogies with the Kuramoto model. Here, the authors analyze a network consisting of parametrically excited nonlinear oscillators and demonstrate that by introducing random interventions, one can promote synchronous collective behavior. Specifically, in the uncoupled limit, the method of averaging is utilized to show that a parametric excitation results in multiple stable steady states. For moderate coupling strengths, this phase space geometry remains largely intact and there exists a multitude of stable steady states. Most of these solutions correspond to asynchronous behavior. In addition, the emergence of cluster synchronization, where multiple clusters of adjacent oscillators with equal phase coexist, is observed. When a weak stochastic input is introduced, the asynchronous behavior is suppressed, and after an initial transient phase, collective behavior is found to emerge. Thus, adding temporal disorder (i.e., noise) to disordered dynamics can generate order (e.g., synchronization). This counterintuitive effect suggests applications in systems ranging from rotating machinery to Josephson junction arrays.

Keywords Disorder · Networks · Synchronization · Parametric excitation · Stochasticity · Coupled oscillators

T. Breunung (✉)
Department of Mechanical Engineering, University of Wisconsin–Madison, Madison, WI 53706, USA
e-mail: breunung@wisc.edu

B. Balachandran (✉)
Department of Mechanical Engineering, University of Maryland, College Park, MD 20742, USA
e-mail: balab@umd.edu

1 Introduction

Synchronization is found to occur when coupled units interact to produce coherent, collective dynamics. This phenomenon is observed in systems as diverse as neurons in biological neural networks [49], generators in power grids [35], reactants in chemical oscillations [23], individuals in social groups [47], and a host of other systems [37]. While applications in mechanical systems have also been reported [31], these applications feature unit dynamics with limit cycle oscillations.

Indeed, based on general averaging arguments, Kuramoto [25] showed that the phase dynamics of weakly coupled limit cycle oscillators can be simplified to a canonical set of equations. These equations are commonly referred to as the Kuramoto model. These gradient dynamical systems have been widely studied (see, e.g., [16,43,44]) and can display various dynamical phenomena such as coherence, decoherence, and chimera states [1]. However, in Kuramoto's analysis, not only perturbations in the radial directions (i.e., the directions normal to the limit cycles), but also coupling between the phase dynamics and radial coordinates are neglected. Thus, the relevance of observations from the abstract Kuramoto model to more realistic systems, such as mechanical oscillators, remains unclear. Furthermore, mechanical oscillators are typically described by non-gradient dynamical systems.

Parametric excitation can also generate self-excited vibrations [37,38]. Parametric excitation occurs when a parameter of the underlying equations of motions is varied in time. This time dependence requires the analysis of a non-autonomous system. By using classical analysis, one can show that an initially stable fixed point can be destabilized by the addition of a weak, periodic parametric excitation to the system [20,50]. A physical realization of this, so called parametric resonance, can be observed in a pendulum with varying base point [21], the traverse vibrations of a beam with pulsating axial load [8,38] or the roll motions of ships [18]. Small networks of parametrically excited networks have been studied in [7,29,42]. Therein, parallels to Ising machines are explored. Since parametrically excited systems (i.e., non-autonomous systems) differ from the cases analyzed by Kuramoto (autonomous systems), it is unclear if observations made using the Kuramoto model carry over to the case of parametrically excited networks.

Most real-world observations of synchronization are made in noisy environments. This motivates researchers to investigate the effects of noise (i.e., temporal disorder) on synchronization. Intuitively, one expects noise to be detrimental to synchronization. Indeed, with the Kuramoto model, it has been found that Gaussian white noise impedes complete synchronization [4]. However, if a single noise term is introduced to act simultaneously on all oscillators, then it was observed that synchronization of uncoupled oscillators is promoted [34]. This observation has been gradually extended to bursting oscillations [39], weakly coupled oscillators [51], and correlated noise [32]. However, it is unclear whether similar observations can be made for non-autonomous mechanical systems.

In this work, the authors study a network of parametrically excited mechanical oscillators, as prototypical non-autonomous, non-gradient dynamical system of coupled nonlinear oscillators. The linear stiffness terms of the unit cells are periodically varied, and this variation results in a Mathieu equation at first order. Additionally, weak coupling between neighboring oscillators and nonlinear restoring forces are introduced. First, the method of averaging is utilized to investigate the unit cell dynamics; that is, the uncoupled limit (cf. Section 2.1). Subsequently, weak coupling is introduced, and dynamics of the full oscillator array is studied. Therein, hyperbolic structures from the uncoupled limit are found to persist and give rise to a multitude of possible steady state solutions (cf. Section 2.2.1). Finally, weak stochastic perturbations are introduced and the order promoting effect of noise for the network is demonstrated (cf. Section 2.2.2).

2 Network of Mathieu-Duffing Oscillators

In this study, the following network of identical oscillators is considered

$$\begin{aligned}&\ddot{q}_j + c\dot{q}_j + (\omega^2 + k_P\cos(\Omega t))q_j\\&\quad +k_3 q_j^3 + k_c(q_j - q_{j-1}) + k_c(q_j - q_{j+1})\\&\quad = \sigma\dot{W}, \quad j = 1, \ldots, N, \end{aligned} \tag{1}$$

with the notation $q_0 = q_N$ and $q_{N+1} = q_1$ implying cyclic boundary conditions. The positive coefficient $c > 0$ is utilized to model linear damping and ω corresponds to the natural frequency. The parameter k_c corresponds to the linear coupling between adjacent oscillators. Furthermore, a parametric excitation is introduced through the term $k_P\cos(\Omega t)q$. This type of parametric stiffness excitation is also present in the classical Mathieu equation [21,41]. The term k_3q^3 is due to a nonlinear restoring force and is the classical Duffing type nonlinearity [20,24,38]. In equation (1), the term on the right-hand side of each oscillator represents a Gaussian white noise term, wherein σ is used to denote the noise intensity and W is used for the standard Wiener process. A similar system without parametric excitation (i.e., $k_P = 0$ in equations (1)) has been used in earlier work on circular oscillator arrays [5].

The noise free system ($\sigma = 0$) has a fixed point at the origin ($q_1 = q_2 = \ldots = q_N = 0$). Without parametric excitation, this equilibrium is stable, due to the presence of dissipation ($c > 0$). If the parametric excitation frequency is tuned appropriately ($2\omega \approx l\Omega$ for $l = 1, 2, \ldots$), a parametric resonance can occur (cf., e.g., [20,21,38]). In this case, the origin becomes unstable, and the system response departs from the origin. The nonlinear restoring force $k_3 q_j^3$ acts to restrict the system's displacements and impedes unbounded growth of the vibration amplitudes. In the following, these arising oscillations are studied.

In the uncoupled limit $k_c \to 0$ of equation (1), the individual coordinates q_j are independent. Hence, in this limit, the dynamics of individual oscillators or unit cells can be studied independently of each other. It is noted that this uncoupled limit is also referred to as anti-continuous limit in studies on spatially localized solutions [3,5,28,30]. In the following, the uncoupled limit is analyzed first. Based on this analysis, the dynamics of the coupled array is subsequently considered.

2.1 Single Cell Dynamics

The equation of motion of a unit cell is obtained by setting $k_c = 0$ in the array system (1), which yields

$$\ddot{q} + c\dot{q} + (\omega^2 + k_P \cos(\Omega t))q + k_3 q^3 = \sigma \dot{W}. \tag{2}$$

First, the single cell dynamics (2) is studied without added Gaussian white noise ($\sigma = 0$). Subsequently, the stochastic term is added ($\sigma > 0$) to understand the impact of this random intervention on the single cell dynamics.

2.1.1 Noise free unit cell dynamics

A small positive parameter ε is introduced as a scaling factor to analyze the single-cell dynamics (2) via perturbation methods. To this end, the limit of weak damping $c \to \varepsilon c$, weak parametric excitation $k_P \to \varepsilon k_P$, and weak nonlinearities $k_3 \to \varepsilon k_3$ of system (2) is considered in equation (2). Moreover, the dimensionless time $\tau = \Omega t$ is introduced and the single cell dynamics (2) can be rewritten in the form

$$q'' + \frac{\omega^2}{\Omega^2} q = -\frac{\varepsilon}{\Omega^2}\left(\Omega c q' + k_P \cos(\tau) + k_3 q^3\right), \quad 0 < \varepsilon \ll 1, \tag{3}$$

where $\square' = d/d\tau$ is the time derivative with respect to the dimensionless time τ. In the next step, the detuning equation $\Omega = \Omega_0 + \varepsilon\Omega_1$ is introduced and a Taylor series expansion of equation (3) in the small parameter ε about $\varepsilon = 0$ is performed. These steps yield

$$\begin{aligned} q'' + \frac{\omega^2}{\Omega_0^2} q &= -\frac{\varepsilon}{\Omega_0^2}\left(\Omega c q' + k_P \cos(\tau) + k_3 q^3 - 2\omega^2 \frac{\Omega_1}{\Omega_0} q\right) \\ &\quad + \mathcal{O}(\varepsilon^2) \\ &= \varepsilon f_1(q, \dot{q}, \tau) + \mathcal{O}(\varepsilon^2) \end{aligned} \tag{4}$$

where the expression $\mathcal{O}(\varepsilon^2)$ denotes terms of order two or higher in the expansion parameter ε. Moreover, the function $f_1(q, \dot{q}, \tau)$ is introduced to denote the first order terms on the right-hand side of equation (4). By substituting the transformation $q(\tau) = u(\tau)\sin(\bar{\omega}\tau) + v(\tau)\cos(\bar{\omega}\tau)$ with $\bar{\omega} = \omega/\Omega_0$ into equation (4) the authors obtain

$$\begin{aligned} u' &= \varepsilon f_1(u\sin(\bar{\omega}\tau) + v\cos(\bar{\omega}\tau), u\bar{\omega}\cos(\bar{\omega}\tau) \\ &\quad - v\bar{\omega}\sin(\bar{\omega}\tau), \tau)\cos(\bar{\omega}\tau) + \mathcal{O}(\varepsilon^2), \\ v' &= -\varepsilon f_1(u\sin(\bar{\omega}\tau) + v\cos(\bar{\omega}\tau), u\bar{\omega}\cos(\bar{\omega}\tau) \\ &\quad - v\bar{\omega}\sin(\bar{\omega}\tau), \tau)\sin(\bar{\omega}\tau) + \mathcal{O}(\varepsilon^2), \end{aligned} \tag{5}$$

which are in the standard from amendable to apply the method of averaging [41,46].

In the following, the authors study the first, or fundamental, parametric resonance, which occurs when the frequency of the parametric excitation Ω is approximately twice that of the natural frequency ω; that is, $\Omega \approx 2\omega$. The small difference between 2ω and Ω is set equal to the detuning parameter Ω_1 (recall the detuning equation $\Omega = \Omega_0 + \varepsilon\Omega_1$). Thus, Ω_0 is set to two times the eigenfrequency ω and the rescaled frequency $\bar{\omega} = \omega/\Omega_0$ is equal to 0.5. For these parameters, the function f_1 is periodic in the dimensionless time τ (cf. equation (4)) and averaging results for periodic systems can be applied to equations (5). Applying the method of averaging to the system (5), the authors obtain the averaged system

$$\begin{aligned} u' &= \frac{\varepsilon}{4\Omega_0^2}\Big(-2\Omega_0 c\, u - 2k_P\, v \\ &\quad + 2\Omega_0\Omega_1\, v - 3k_3\,(u^2 v + v^3)\Big), \\ v' &= \frac{\varepsilon}{4\Omega_0^2}\Big(-2\Omega_0 c\, v - 2k_P\, u \\ &\quad - 2\Omega_0\Omega_1\, u + 3k_3\,(u v^2 + u^3)\Big), \end{aligned} \tag{6}$$

which governs the time evolution of the amplitudes $u(\tau)$ and $v(\tau)$ on the slow time scale $\varepsilon\tau$. The error between the approximation (6) and the full system (3) is of order one in the small parameter ε for long time

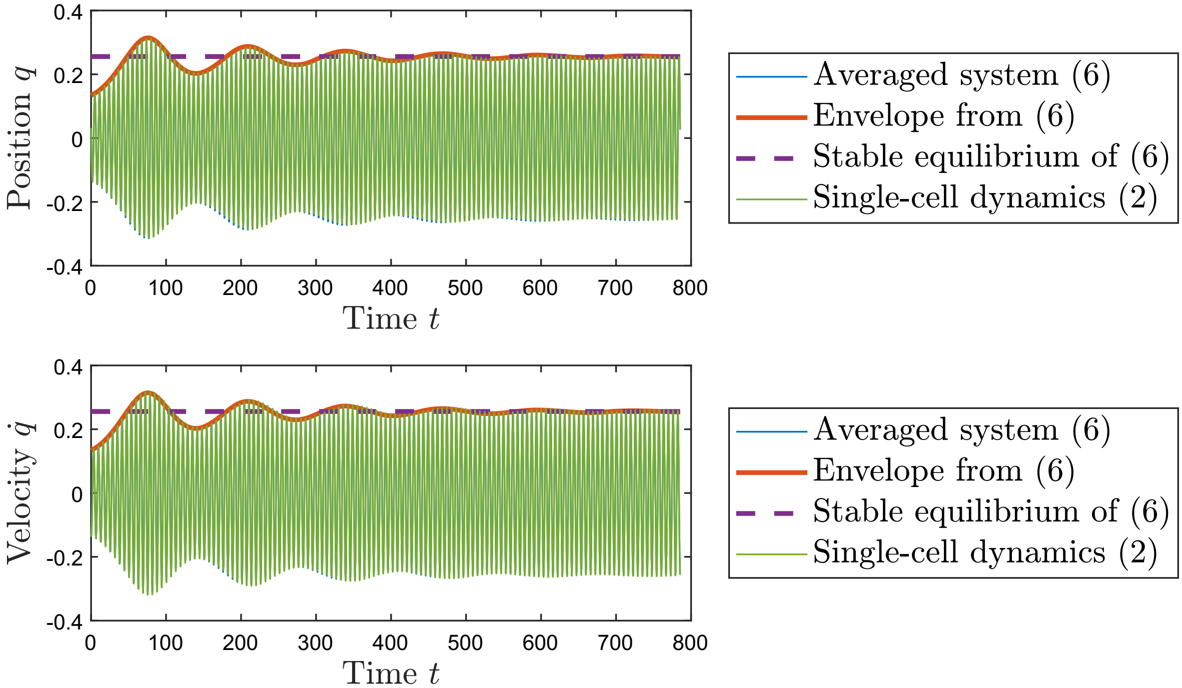

Fig. 1 Solution of the averaged system (6) and the full system (2) for the parameter values $c = 0.01$, $\omega = 1$, $k_3 = 1$, $k_P = 0.1$, $\Omega = 2 = 2\omega$, and $\sigma = 0$

scales $1/\varepsilon$. Higher order formulae and more details on averaging can be found, for example, in references [41, 46].

To illustrate the accuracy of the dynamics of the averaged system (6), this system is solved via numerical time integration[1] for the parameter values $\omega = 1$, $c = 0.01$, $k_3 = 1$, and $k_P = 0.1$. Subsequently, the resulting time series of the slow variables $u(\tau)$ and $v(\tau)$ are transformed back to obtain the position q and velocity $\dot{q}$. The resulting time series are shown in Fig. 1. In addition to solutions of the averaged system (6), numerical solutions of the full system (2) are included in Fig. 1. It is found that both solutions agree well without any discernible difference. Moreover, the envelope obtained from the averaged dynamics (6) is included in Fig. 1.

In addition to solutions obtained by numerical time integration of the averaged system (6), the averaged system (6) can be solved for fixed points. Introducing the notation

$$\Xi_1 = \frac{k_P^2 + k_P\Omega_0\Omega_1 - c^2\Omega_0^2}{3k_P k_3},$$
$$\Xi_2 = \frac{1}{3k_P k_3}\sqrt{(k_P^2 - c^2\Omega_0^2)(k_P + \Omega_0\Omega_1)^2}, \tag{7}$$

the fixed points of the averaged system (6) are found to be given by

$$u^{(1)} = 0, \quad u^{(2,3)} = \pm\sqrt{\Xi_1 - \Xi_2},$$
$$u^{(4,5)} = \pm\sqrt{\Xi_1 + \Xi_2},$$
$$v^{(j)} = \frac{-2k_P^2 u^{(j)} + c^2\Omega_0^2 u^{(j)} - 2k_P\Omega_0\Omega_1 u^{(j)} + 3k_P k_3 (u^{(j)})^3}{ck_P\Omega_0 + c\Omega_0^2\Omega_1},$$
$$j = 1, 2, \ldots, 5, \tag{8}$$

where only real solutions $u^{(j)}$ and $v^{(j)}$ are valid. As indicated in equation (8), up to five fixed points can coexist for the averaged dynamics (6).

The stability of the fixed points (8) can be assessed by computing the eigenvalues of the Jacobian matrix $\mathbf{J}(u, v)$ of the averaged system (6), which is given by

[1] The authors employ MATLAB's routine `ode45`.

$$\mathbf{J}(u, v) = \frac{\varepsilon}{4\Omega_0^2} \begin{bmatrix} -2c\Omega_0 - 6k_3uv & -2k_P + 2\Omega_1\Omega_0 - 3k_3u^2 - 9k_3v^2 \\ -2k_P - 2\Omega_1\Omega_0 + 9k_3u^2 + 3k_3v^2 & -2c\Omega_0 + 6k_3uv \end{bmatrix}. \tag{9}$$

The stability type of the fixed point $(u^{(j)}, v^{(j)})$ is determined by the maximal real part of the eigenvalues of the Jacobian $\mathbf{J}(u^{(j)}, v^{(j)})$; that is, $\mathrm{Re}_{\max} := \max(\mathrm{Re}(\mathrm{eig}(\mathbf{J}(u^{(j)}, v^{(j)}))))$. If $\mathrm{Re}_{\max}$ is positive, then the fixed point $(u^{(j)}, v^{(j)})$ of the averaged dynamics (6) is unstable. If, on the other hand $\mathrm{Re}_{\max}$ is below zero, then the corresponding fixed point $(u^{(j)}, v^{(j)})$ is stable. If $\mathrm{Re}_{\max}$ is equal to zero, then the stability analysis in inconclusive and higher order perturbations need to be employed to determine the stability of the fixed point $(u^{(j)}, v^{(j)})$.

The fixed points $(u^{(j)}, v^{(j)})$ correspond to periodic solutions for the system (4). In Fig. 1, one can discern that the solution of the single-cell system (2) quickly settles to the stable steady state (8) of the averaged system (6). Obtaining the averaged dynamics allows one to compute the steady state in closed form, while deducing the steady state solutions and the associated stability directly from the full system (2) requires numerical techniques.

The fixed points of the averaged system (6) depend on the frequency of parametric excitation Ω. This dependence is depicted in Fig. 2 for the parameter values $c = 0.01$, $\omega = 1$, $k_3 = 1$, and $k_P = 0.1$. It is observed that the origin of system (2) is stable except when the frequency of the parametric excitation Ω is close to two, which is twice that of the natural frequency ω. For parametric excitation frequencies Ω below 1.95, the dynamics of the averaged system (6) is found to feature a single stable fixed point at the origin (gray inset in Fig. 2). At $\Omega = 1.95$, a supercritical pitchfork bifurcation of the origin is observed in the dynamics of the averaged system (6). The equilibrium point at the origin is found to loose stability and two stable fixed points are found to emerge in the averaged dynamics (cf. orange inset in Fig. 2).

For $\Omega = 2.05$, a subcritical pitchfork bifurcation of the trivial fixed point is found to occur in the averaged system (6). Consequently, the origin point of the averaged dynamics (5) becomes stable again and two unstable fixed points emerge. Together with the two stable fixed points emerging from the supercritical pitchfork bifurcation at $\Omega = 1.95$, five fixed points coexist for parametric excitation frequencies exceeding 2.05 (cf. magenta inset in Fig. 2).

The occurrence of pitchfork bifurcations at the origin of the averaged system (6) can be supported by the following general argument. First, it is noted that at most, the center manifold at the origin has dimension one. Indeed, the divergence of the linearization of the right-hand side of the averaged system (6) at the origin is negative. This indicates a local contraction of phase space volumes. Thus, at the origin the slow flow (6) must contract at least along one direction. This leaves only one remaining direction along which one can have a center manifold. Moreover, due to the absence of even terms in the averaged system (6), the observed bifurcations are generically pitchfork bifurcations.

The analytical solutions obtained for the averaged dynamics are verified by carrying out a numerical continuation study of the unit cell dynamics (2) by using the software package COCO [15]. These solutions are also included in Fig. 2, and overall, a good agreement is observed. Only for large parametric excitation frequencies (i.e., $\Omega > 2.5$) and large amplitudes, the amplitudes computed from the averaged system (6) are found to deviate from the numerical solution of the full system (2). This is to be expected, since within the averaging procedure, it is assumed that the frequency of parametric excitation Ω is close to two (i.e., $\Omega \approx 2\omega$). Nevertheless, the overall phase space behavior obtained from the averaged system (6) (i.e., three stable and two unstable steady states) remains accurate.

Within Fig. 2, the equilibrium solutions determined for a fixed value of the parametric excitation amplitude k_P (i.e. $k_P = 0.1$) is displayed. One of these equilibrium solutions is the origin included in Fig. 2. The stability of this fixed point corresponds to a horizontal line in the Ince-Strutt diagram (cf., e.g., [21,37,38]) for the linearization of equation (3) at the origin. For positive, non-zero damping $c > 0$ the instability regions of the Ince-Strutt diagram detach from the lines $k_P = 0$. Thus, for very small amplitudes of the parametric excitation k_P, no bifurcations will be observed and the origin of system (2) is stable for all frequencies of parametric excitation Ω_P. For larger amplitudes of the para-

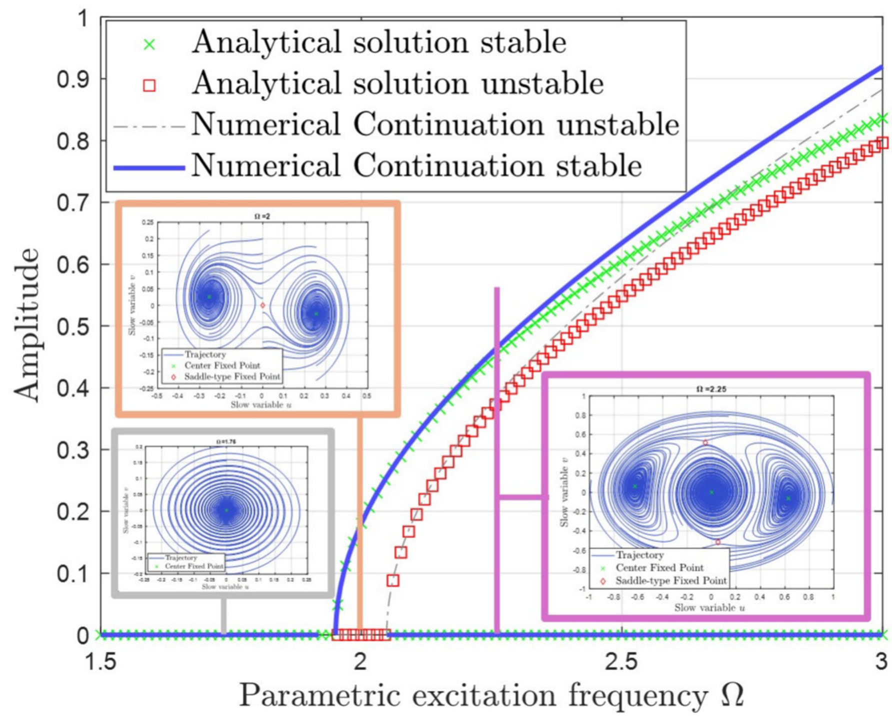

Fig. 2 Equilibrium solutions of the unit cell system (2) for the parameter values $c = 0.01$, $\omega = 1$, $k_3 = 1$, $k_P = 0.1$, and $\sigma = 0$. Results from the averaged system (6) are compared with those obtained from a numerical continuation study of the unit cell dynamics (2).

metric excitation k_P, the bifurcation diagram for varying frequency of parametric excitation is qualitatively similar to Fig. 2. Furthermore, it is noted that the perturbation analysis is restricted to the limit of weak parametric excitation and the vicinity of the first parametric resonance.

After discussing the phase space geometry of the unit cell without noise, weak or low-level noise is added to the unit cell dynamics and the resulting dynamics is discussed in the following section.

2.1.2 Single cell system with noise

Based on earlier work [5,12,19] it is expected, that for small noise intensities $0 < \sigma \ll 1$, the deterministic dynamics of the unit cell discussed in the previous section will strongly influence the stochastic dynamics. More specifically, realizations of the arising stochastic differential equation remain in the vicinity of the stable attractors of the deterministic system and occasionally jump between the coexisting stable attractors [19,33].

For the frequency of parametric excitation Ω equal to two ($\Omega = 2$) and the parameter values $c = 0.01$, $\omega = 1$, $k_3 = 1$, and $k_P = 0.1$, two stable steady states for the noise free ($\sigma = 0$) single cell dynamics are observed (cf. orange inset in Fig. 2). The corresponding stable fixed points of the averaged dynamics are given by

$$u^{(4,5)} = \pm 0.2542, \qquad v^{(4,5)} = \mp 0.0257. \tag{10}$$

The arising attractors of the single cell dynamics (2) in the vicinity of the solutions of the averaged equations are labeled as 4 and 5, respectively.

The addition of noise causes trajectories to transition between these attractors. For example, a trajectory initialized at attractor 4 first remains in the vicinity of attractor 4, and then, after a while escapes to attractor 5. The mean time until the first exit from the vicinity of an attractor is denoted as mean escape time. In the following, the mean escape time is obtained by numerical integration of the stochastic differential equation (2) with the stochastic integration scheme proposed in earlier work [9]. Two hundred samples are initialized at each attractor and the escape time of each sample is extracted. To this end, the time instance that a sample is closer to another attractor than the attractor is initially initialized from is denoted as the escape time. Averaging the escape times for all samples yields an estimate of the mean escape time. The mean escape times for both attractors are shown in Fig. 3. Both escape times

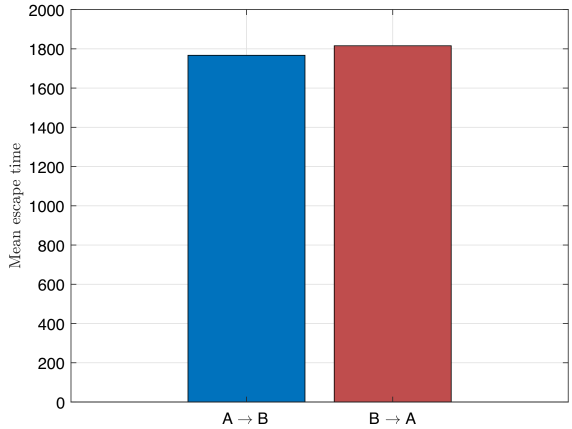

Fig. 3 Bar plot to show the mean escape times for the two attractors of unit cell system (2) with the parameter values $c = 0.01$, $\omega = 1$, $k_3 = 1$, $k_P = 0.1$, $\Omega = 2$, and $\sigma = 0.01$.

are practically equal. This indicates that trajectories can be found in the vicinity of attractor 4 with the same likelihood as those in the vicinity of attractor 5. Neither of the attractors is favored through the addition of weak Gaussian white noise or weak random interventions.

The equality of the two mean escape times can also be expected based on the symmetries of the underlying dynamical system and stochastic processes. To this end, the state space coordinates $\mathbf{x} = [q, \dot{q}]^\top$ are introduced to rewrite the single cell dynamics into the first order form

$$\dot{\mathbf{x}} = \frac{\mathrm{d}}{\mathrm{d}t}\begin{bmatrix} q \\ q \end{bmatrix} = \begin{bmatrix} \dot{q} \\ -c\dot{q} - (\omega^2 + k_P \cos(\Omega t))q - k_3 q^3 \end{bmatrix} + \sigma \begin{bmatrix} 0 \\ 1 \end{bmatrix} \dot{W} = \mathbf{f}(\mathbf{x}, t) + \sigma \mathbf{g}(\mathbf{x}, t)\dot{W}. \tag{11}$$

In the first order system (11), the function $\mathbf{f}(\mathbf{x}, t)$ corresponds to the deterministic dynamics and is also denoted as drift. The term $\mathbf{g}(\mathbf{x}, t)$ is also denoted as diffusion term. From equation (11), one can see that the drift $\mathbf{f}(\mathbf{x}, t)$ has an odd symmetry with respect to the coordinates $\mathbf{x}$; that is, $\mathbf{f}(-\mathbf{x}, t) = -\mathbf{f}(\mathbf{x}, t)$ holds of all times. Thus, if $\mathbf{x}^*(t)$ is a solution for the deterministic dynamics, then $-\mathbf{x}^*(t)$ is also a solution to the deterministic dynamics. This symmetry can also be observed for the fixed points given in equations (8) and (10).

This symmetry carries over to the stochastic case. Given a realization $\mathbf{x}_t(\omega^*)$ of the stochastic dynamical system (11), where ω^* denotes the specific realization of the Gaussian white noise process in equation (11), then $-\mathbf{x}_t(-\omega^*)$ is also a realization the stochastic system (11). Moreover, the probability to observe $\mathbf{x}_t(\omega^*)$ or $-\mathbf{x}_t(-\omega^*)$ are exactly equal, since the probability density of Gaussian white noise is symmetric. Thus, if the realization $\mathbf{x}_t(\omega^*)$ escapes from attractor $\mathbf{x}_4$ at t_4, then there is an equal likely trajectory $-\mathbf{x}_t(-\omega^*)$ escaping from attractor $\mathbf{x}_5 = -\mathbf{x}_4$ at the same time t_4. Hence calculating the mean of all escape times t_4 yields not only an escape time from the attractor $\mathbf{x}_4$ but also the same estimate for the mean escape time from the attractor $\mathbf{x}_5$. This argument holds irrespective of the number of attractors in the system (11). More specifically, it also applies when five steady states coexist for excitation frequencies $\Omega > 2.05$ (cf. Fig. 2). Also in this case, the mean escape times for the non-trivial, stable steady states are equal. More generally, this symmetry argument allows one to conclude that for any parameter selection, steady state solutions are symmetric and that the escape times of two symmetric steady state solutions are equal.

The analysis of the single cell system (2) in the preceding two sections serves as a basis to understand the dynamics of the full array (1). Indeed, the dynamics of the single-cell system (2) is directly relevant for the uncoupled or anti-continuous limit ($k_c \to 0$) of the full array (1) and continues to be relevant for moderate coupling strength $k_c > 0$ as discussed in the next section.

2.2 Array Dynamics

For weak coupling ($k_c > 0$), hyperbolic features of the single cell dynamics determined from (2) continue to exist for the full array (1). Thus, the understanding gained by analyzing the single cell dynamics helps in assessing the more complex dynamics of the full array (1). In the following, the array dynamics without noise (i.e., $\sigma = 0$ in equation (1)) is investigated first. Subsequently, the array dynamics (1) with Gaussian white noise addition is considered.

2.2.1 Noise free array dynamics

The equilibria of the single cell dynamics shown in Fig. 2 are hyperbolic fixed points. Thus, from the implicit function theorem (cf., e.g., [26]), it follows that these equilibria continue to exist and are of the same stability type for small coupling coefficients $0 < k_c \ll 1$.

To study the array dynamics in more detail, the averaging procedure from Section 2.1.1 is repeated for the full array (1). In absence of stochastic forcing $\sigma = 0$ and in the limit of weak damping $c \rightarrow \varepsilon c$, weak parametric excitation $k_P \rightarrow \varepsilon k_P$, weak nonlinearities $k_3 \rightarrow \varepsilon k_3$, and weak coupling $k_c \rightarrow \varepsilon k_c$ the resulting averaged system is given by

$$\begin{aligned} u_j' &= \frac{\varepsilon}{4\Omega_0^2}\Big(-2\Omega_0 c\, u_j - 2k_P\, v_j + 2\Omega_0\Omega_1\, v_j \\ &\quad - k_c(v_j - v_{j+1}) - k_c(v_j - v_{j-1}) \\ &\quad - 3k_3\,(u_j^2 v_j + v_j^3)\Big), \\ v_j' &= \frac{\varepsilon}{4\Omega_0^2}\Big(-2\Omega_0 c\, v_j - 2k_P\, u_j - 2\Omega_0\Omega_1\, u_j \\ &\quad - k_c(u_j - u_{j+1}) - k_c(u_j - u_{j-1}) \\ &\quad + 3k_3\,(u_j v_j^2 + u_j^3)\Big), \quad j = 1, .., N, \end{aligned} \tag{12}$$

where the amplitudes u_j and v_j are associated with the j-th oscillator; that is, $q_j = u_j(\tau)\sin(\bar{\omega}\tau) + v_j(\tau)\cos(\bar{\omega}\tau)$.

To solve for the fixed points of the averaged array system (12), a set of $2N$ nonlinear equations needs to be solved. In the absence of closed form solutions, a numerical continuation strategy is pursued as follows. From the analysis of Section 2.1.1, specifically, equation (8) is used to obtain the fixed points of the averaged system (12) for zero value of the coupling k_c. These initial solutions can be now numerically continued for $k_c > 0$ utilizing sequential continuation. To this end, the coupling strength k_c is incrementally increased $k_c^{(l)} \rightarrow k_c^{(l+1)}$ and the averaged dynamics are solved numerically for a fixed point [2]. Therein, the fixed point for the previous coupling strength $k_c^{(l)}$ is supplied as an initial guess to ensure that the new fixed point for $k_c = k_c^{(l+1)}$ is a close continuation of the fixed point for $k_c = k_c^{(l)}$. This procedure is repeated until a final value for k_c is reached. An outcome of such numerical continuation procedure is depicted in Fig. 4. Therein, the norm of the fixed points of the averaged system (12) is shown for an array consisting of ten oscillators ($N = 10$).

For the parameter values $c = 0.01$, $\omega = 1$, $k_3 = 1$, $k_P = 0.1$, $\Omega = 2$, and $\sigma = 0.01$, three steady state solutions exist for each unit cell (cf. Fig. 2). While the origin is unstable, the two fixed points of the averaged unit cell dynamics given in equation (10) are stable. This implies that for the uncoupled array ($k_c = 0$) $59049 = 3^{10} = 3^N$ steady state solutions exist for the full array, out of which $1024 = 2^{10} = 2^N$ are stable. For all of the stable solutions, the amplitudes u_j and v_j are respectively either at $u^{(4)}$ and $v^{(4)}$ or $u^{(5)}$ and $v^{(5)}$ (cf. equation (10)). Thus, the amplitudes of the stable solutions only differ in their sign and have the same magnitude; that is, $|u_j| = |u_l|$ and $|v_j| = |v_l|$. This implies that all stable fixed points of the averaged system have the same norm in the uncoupled limit ($k_c = 0$) and hence collapse into a single point in the visualization shown in Fig. (4). For the other fixed points, the amplitudes u_j and v_j of at least one oscillator j are zero, rendering the corresponding fixed point unstable and moreover decreasing the magnitude of the associated norm (cf. Fig. 4).

With increased coupling spring constant k_c, the norms of these fixed points change (cf. Fig. 4). While the magnitudes of the norms associated with most of the fixed points decrease, the magnitudes of the norms of two stable steady states and the unstable fixed point at the origin remain unchanged. The origin remains an unstable fixed point of the averaged system (12) irrespective of the coupling. The stable fixed points correspond to the solution where the amplitudes u_j and v_j of all oscillators have the same sign; that is, $u_j = u^{(4,5)}$ and $v_j = v^{(4,5)}$. Since, the averaged system (12) or the full system (1) are only impacted by the difference in the position of adjacent oscillators (i.e., $q_j - q_{j+1}$ and $q_j - q_{j-1}$ in equation (12)), these two fixed points remain unaltered by the introduction of coupling between the oscillators. The norm magntiudes other fixed points decrease and many of those, stable and unstable, disappear through pitchfork bifurcations. For the example shown in Fig. (4) and the coupling strength $k_c = 0.1$, 10655 unique fixed points[3] exist, while 59049 fixed points are found for the uncoupled array dynamics ($k_c = 0$). Moreover, the number of stable fixed points has decreased to 322 from initially 1024 stable fixed points.

While for two stable steady states (i.e., the two steady states with constant norm in Fig. 4) the masses oscillate synchronously, this behavior is not observed for the other fixed point of the averaged system (12).

[2] The authors have employed MATLAB's routine `fsolve`.

[3] Two fixed points are numerically distinguished if their relative distance; that is, the distance between the two fixed points divided by the norm of one of the fixed points, is larger than 0.1.

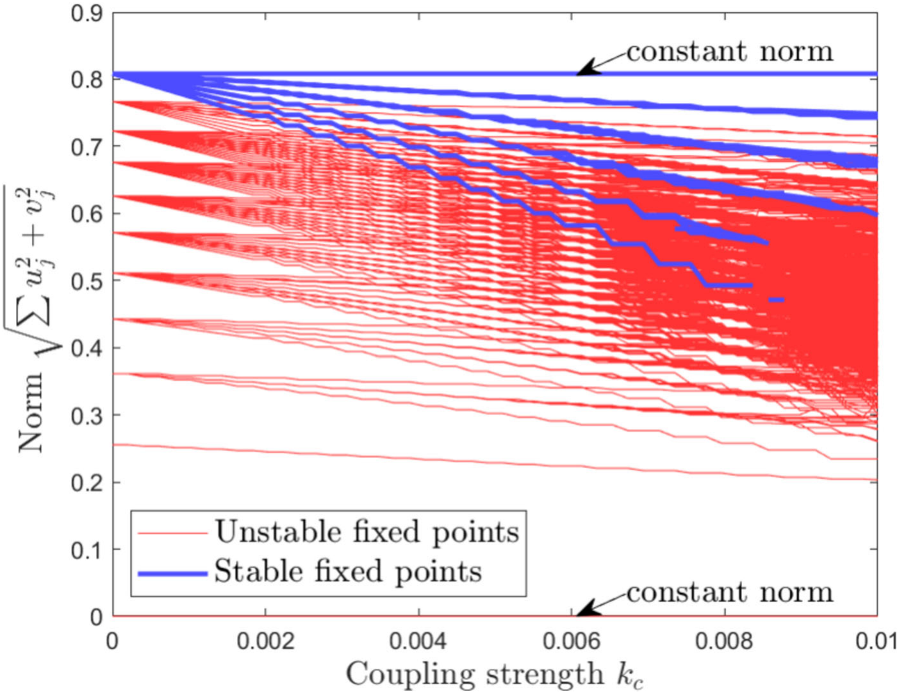

Fig. 4 Norm of the fixed points of the averaged system (12) with ten oscillator ($N = 10$) plotted with respect to the coupling strength k_c. The parameter values are $c = 0.01$, $\omega = 1$, $k_3 = 1$, $k_P = 0.1$, and $\Omega = 2$

To illustrate this behavior, the phases of the individual oscillators are defined as follows

$$\phi_j = \tan^{-1}\left(\frac{q_j}{\dot{q}_j}\right), \tag{13}$$

where the four-quadrant inverse tangent (also referred to as atan2) is utilized. The phase alignment of the individual oscillators is commonly quantified via the order parameter r [25,43], defined as follows:

$$r = \left|\frac{1}{N}\sum_{j=1}^{N} \mathrm{e}^{\mathrm{i}\phi_j}\right|, \tag{14}$$

where $\mathrm{i} = \sqrt{-1}$ is used to denote the imaginary unit. For varying coupling stiffness values, the order parameters of the stable steady states of the averaged system (12) for varying coupling stiffness are shown in Fig. 5. Therein, it is discernible that the order parameter takes the five distinct values $r = \{0, 0.2, 0.4, 0.6, 0.8, 1\}$. For the uncoupled limit (i.e., $k_c = 0$), this behavior can be explained as follows. For $r = 1$, all oscillators are in synchrony; that is, all oscillators are at the steady state close to $u^{(4)}$ and $v^{(4)}$, or alternatively all oscillators are at the steady state close to $u^{(5)}$ and $v^{(5)}$ (cf. blue inset in Fig. 5). These two states correspond to perfect synchronization. If nine oscillators are close to attractor 4 and one close to attractor 5, or alternatively one close to attractor 4 and nine close to attractor 5, then the order parameter takes the value 0.8 (cf. orange inset in Fig. 5). Similarly, $r = 0.6$ corresponds to eight oscillators close to attractor 4 and two close to attractor 5, or alternatively two close to attractor 4 and eight close to attractor 5 (cf. green inset in Fig. 5). For $r = 0$, the oscillators are equally distributed between the two attractors of the uncoupled limit; that is, five oscillators are close to the state 4 and the other five oscillators are close to the steady state 5 (cf. gray inset in Fig. 5).

For non-zero coupling ($k_c > 0$), the perfectly synchronized solutions ($r = 1$) remain unchanged as discussed earlier. Hence, their associated order parameter r remains constant at one. For the non-synchronized, stable solutions (i.e., $r < 1$), the order parameter r remains constant as well (cf. Fig. 5), although the individual response trajectories of the oscillators are impacted by the coupling.

The initial condition will determine which of the multitude of stable solutions shown in Fig. 4 are observed. Trajectories launched from random initial conditions could in principle be attracted towards one

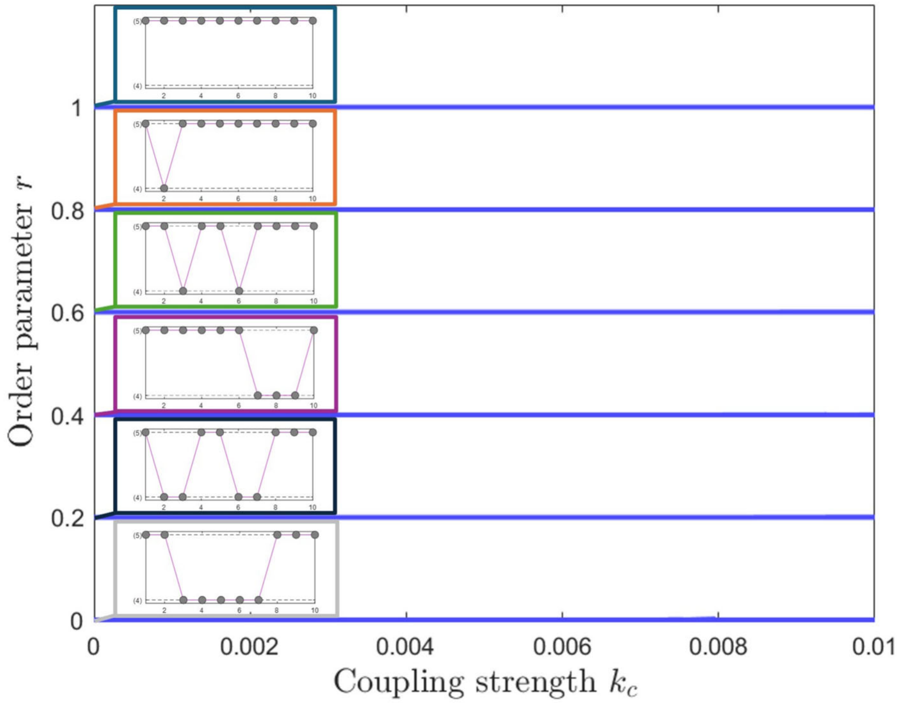

Fig. 5 Order parameter r for the stable steady states of the averaged system (12) with ten oscillators ($N = 10$) for varying coupling strength k_c. The parameter values are $c = 0.01$, $\omega = 1$, $k_3 = 1$, $k_P = 0.1$, and $\Omega = 2$. The insets are meant to illustrate a possible steady state associated with the corresponding order parameter

of the two synchronized solutions, but it seems more likely that another, not-synchronized solutions with $r < 1$ will be observed. This question and the influence of added noise on the observed trajectories will be discussed in the next section.

2.2.2 Array dynamics with added noise

In the preceding section, it is shown that many stable steady state solutions arise in the dynamics of the full array (1). The initial condition will determine the steady state that is observed. To illustrate this point, an array with one hundred oscillators ($N = 100$) and the parameters $c = 0.01$, $\omega = 1$, $k_3 = 1$, $k_P = 0.1$, $\Omega = 2$, and $k_c = 0.1$ is considered. The initial conditions of the array are set to $q_j(0) = 0.001 \sin(\varphi_j)$ and $\dot{q}_j(0) = 0.001 \cos(\varphi_j)$, where the initial phases φ_j are sampled from the uniform distribution within the interval between 0 and 2π. This choice of the initial condition yields a random initial order parameter r for the array (1). On the left side of Fig. 6a, the phases after 2000 periods of ten sample trajectories without noise (i.e., $\sigma = 0$) are shown. For each trial number l, the phases are scaled to be within the interval between -0.5 and 0.5, and then the trial number l is added. This approach yields the ten distinguishable curves shown in Fig. 6a. Overall, it is discernible that the phases of the oscillators are not aligned. Rather one or more populations of adjacent oscillators with the same phases (i.e., $\phi_j = \phi_{j+1} = \phi_{j+2} = ... = \phi_{j+l} \neq \phi_{j+l+1} = \phi_{j+l+2} = ...$) are observed. This phenomenon is denoted as cluster synchronization and has been observed in a wide range of systems [40,45].

It is noted that the solutions q_j and $\dot{q}_j$ in Fig. 6ahave reached a periodic steady state. Along these solutions, the individual phases evolve in time $\phi_j = \Omega t + \phi_j^*$. Thus, selecting a different, but large enough, final time would shift all individual phases shown in Fig. 6aby the same constant angle. This shift would not alter the order parameter r and the distributions of the individual clusters. Both, the order parameter r and the distributions of the clusters have reached a steady state.

The individual clusters of synchronization impede a complete synchronization of the array. After conducting a simulation of the same oscillator configuration with added noise of intensity $\sigma = 0.005$, the obtained final phases shown on the right of Fig. 6a. It is observed that the phases of the one hundred oscillators for all ten trials are perfectly aligned. Thus, in all cases, synchronization is generated by the addition of Gaussian white noise.

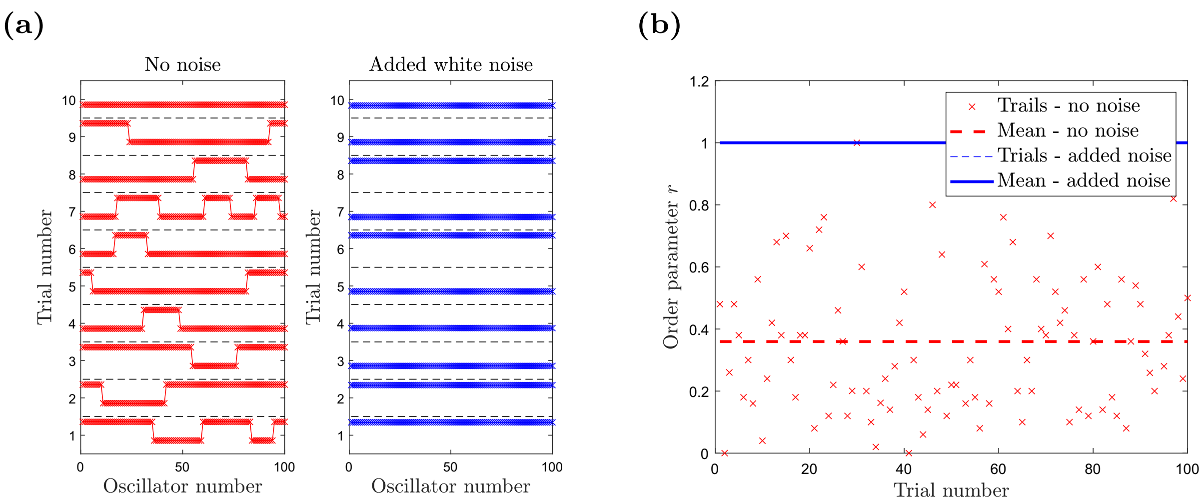

Fig. 6 Array dynamics (1): a) Final phases (i.e., after 2000 periods) of the individual oscillators without added Gaussian white noise (left) and with added Gaussian white noise (right).b) Order parameter r. Parameter values $c = 0.01$, $\omega = 1$, $k_3 = 1$, $k_P = 0.1$, $\Omega = 2$, $k_c = 0.1$, $\sigma = 0.005$, and $N = 100$

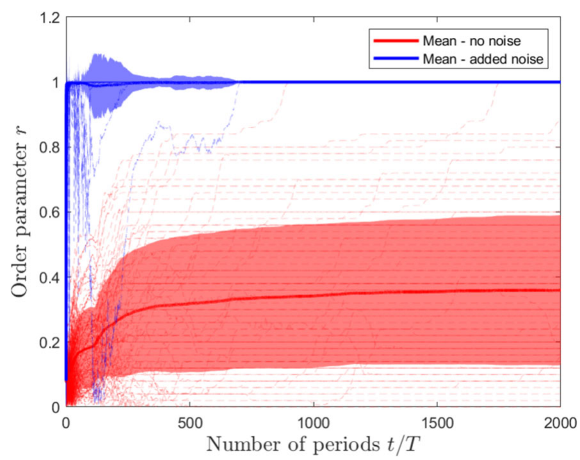

Fig. 7 Order parameter r for the oscillator array (1) without ($\sigma = 0$) and with added Gaussian white noise ($\sigma = 0.005$). The parameter values are $c = 0.01$, $\omega = 1$, $k_3 = 1$, $k_P = 0.1$, $\Omega = 2$, $k_c = 0.1$, and $N = 100$

To further illustrate the synchronization promoting characteristic of the added Gaussian white noise, the order parameter r of solutions with and without added noise are computed and shown in Fig. 6b. For the noise free case, the order parameter r is significantly below one. Thus, only partial synchronization is observed. Without added noise, the order parameter is 0.4 on average for the one hundred computed trials. On the other hand, when weak Gaussian white noise with an intensity $\sigma = 0.005$ is introduced into the array dynamics, the order parameter r is raised to one for all trials. Thus, a perfect synchronization is achieved in all cases. From this numerical experiment, it is noted that the addition of noise can be utilized to promote synchronization in networks of parametrically excited oscillators.

Furthermore, the time evolutions of the order parameter r for the array without added noise and with added noise are shown in Fig. (7). Therein, the mean of one hundred samples (solid lines) as well as the standard deviation (shaded regions surrounding the mean) are included. Furthermore, the light lines are used to indicate individual samples. It is discernible that through the addition of the Gaussian white noise the order parameter quickly approaches one for all samples. In many cases, a perfect synchronization is already reached after 100 periods. For 700 periods, all samples have reached perfect synchronization, and the standard deviation of the order parameter r is zero. For the samples without added noise (red in Fig. (7)), the order parameter r is found to initially increase but reaches one only for a few samples. For most samples, this parameter remains at a constant value below 0.8. Thus, on average, the order parameter r remains at 0.4 (cf. also Fig. 6b), which indicates that there is no complete synchronization. Rather, a cluster synchronization is observed (cf. 6a).

The observations from Fig. 6 and Fig. 7 can be confirmed for a variety non-zero and positive damping values c. However, the damping value needs to be small enough, or alternatively the amplitude of the parametric excitation k_P needs to be strong enough so that the origin of the array (1) becomes unstable and non-trivial dynamics can be observed.

The observations made from Figs 6 and 7 indicate that the synchronized states dominate the steady state behavior of the stochastically perturbed array. For the weak noise case, this behavior can be framed in the context of experiments and simulations for similar systems [2,5,9,10] and the large deviation theory [19][4]. Theory, experiments, and simulations strongly suggest that the dominating transition to the synchronized steady state can be observed for different noise intensities, alternative noise models (e.g., colored noise), and a wide variety of coupling strengths. Moreover, according to the theory prediction, noise induced transition towards the synchronized attractors of the deterministic dynamics will invariably occur for any weak noise intensity ($0 < \sigma \ll 1$). The time to observe noise-induced transition to the synchronized steady states decreases exponentially with increasing noise intensity σ and is governed by the quasi-potential [19], which is a functional relying on the deterministic dynamics of the array (1). However, computations of the quasi-potential are challenging even for low dimensional systems (cf, e.g., [14]).

3 Concluding Remarks

The dynamics of a network of parametrically excited, identical nonlinear oscillators is examined in this study. The analysis is started from the uncoupled or anti-continuous limit ($k_c = 0$), wherein the oscillators are independent from each other. In this limit, the method of averaging is utilized to obtain simplified equations of motion (6). From an analysis of the associated slow dynamics, it is found that several fixed points exist (cf. equation (8)). Moreover, it is revealed that for increasing frequency of parametric excitation, the origin undergoes a supercritical pitchfork bifurcation and a subcritical pitchfork bifurcation (cf. Fig. 2). By introducing noise into a unit oscillator with two coexisting stable steady states, it is observed that the mean escape time of the stable, non-trivial attractors are equal, implying that the trajectories are equally distributed in the neighborhood of the two attractors (cf. Fig. 3).

The coexisting equilibria in the averaged system for a single cell give rise to many coexisting periodic solutions in the dynamics of the full array. More specifically, the hyperbolic solutions obtained in the uncoupled limit ($k_c = 0$) continue to exist for the weakly coupled array ($k_c > 0$). This results in a multitude of steady state solutions, which grows exponentially with the number of oscillators N. For the overwhelming majority of these solutions, the oscillator responses are not synchronized. Thus, without noise, it is observed that the trajectories settle towards steady states in which the oscillators are not synchronized (cf. Fig. 6a). Moreover, cluster synchronization; that is, patterns of populations of adjacent oscillators with equal phase, are observed. Finally, Gaussian white noise is introduced into the full array dynamics, and it is observed that the phases of the individual oscillators are synchronized (cf. Fig. 6b). This finding means that one can harness temporal disorder (i.e., noise) to promote order in a network of coupled oscillators.

The underlying equations of motion of the array are motivated by an application in rotating machinery. Indeed, cyclic models similar to the oscillator array (1) are often employed to gain fundamental understanding or quantitative modeling of a bladed disks in turbine engines [13]. Thus, it is expected that the order promoting effect of noise can be utilized in such applications. Experimental investigations are currently underway. In applications, it will be crucial to introduce a well-controlled parametric excitation. For rotating machinery, an approach could be based on exploiting the influence of the rotation speed on the blade stiffness; that is centrifugal stiffening [22,27]. Thus, in principle, a periodic variation of the rotor speed could be utilized to generate to a parametric excitation.

Additionally, applications to Josephson junction arrays are suggested. Indeed, synchronization in arrays of Josephson junctions have been observed [48]. However, therein the effects of the capacitance are

[4] Strictly speaking, it remains unclear if the theory developed by Freidlin and Wentzell [19] applies to the dynamics of the array (1). One underlying reason is that the noise used in the array dynamics (1) is degenerate. This degeneracy stems from the fact that the noise acts only on the position coordinates in the first order form (11), and hence the diffusion matrix $\mathbf{g}(\mathbf{x})\mathbf{g}^\top(\mathbf{x})$ is singular. However, the extension of the large deviation theory to for degenerate diffusion matrices has been conjectured in the physics and engineering literature [11,14,17].

neglected. For non-negligible capacitance, the dynamics of the wave-function difference is a second order differential equation, which is similar to the array dynamics (1) (cf., e.g., [6]). Thus, the observed synchronization promoting impact of Gaussian white noise could also be utilized to enhance synchronization in arrays of Josephson junctions.

The utilized array dynamics (1) is based on several simplifying modeling assumptions and actual physical realizations will depart from this idealization. For example, while it is assumed that the parameters of each oscillator are identical, the effects of mistuning between the oscillators similar to the previous studies [48] could be considered in the future. The temporal disorder studied here may be used to overcome disorder in parameters and other system aspects, akin to a previous study on semi-conductor diode arrays described by an autonomous system [36]. Similarly, it is assumed that a single white noise term acts on all oscillators simultaneously in the array (1). While this corresponds to the case where the whole array is subjected to a single noise source, multiple noise sources, potentially spatially correlated, could be considered in sequential studies. In the same vein, the noise acting on the array could be selected to be non-Gaussian. In applications where it is planned to harvest the noise directly from the array environment, the noise will be non-Gaussian. While most of the discussed observations in the article are robust to changes in the parameter and hence remain relevant for moderate deviations from the idealized array dynamics (1), it remains important to quantify the impacts of these factors in future studies.

Author contributions T.B. and B.B. reviewed the literature and designed the research. T.B. carried out the computations and T.B. and B.B. analyzed and discussed the results. T.B. and B.B. wrote the paper.

Funding The authors gratefully acknowledge the support received through the ONR MURI Grant No. N00014-24-12547 and the Minta Martin Professorship.

Data Availability No datasets were generated or analysed during the current study.

Declarations

Competing interests The authors declare no competing interests.

References

1. Abrams, D.M., Strogatz, S.H.: Chimera states for coupled oscillators. Phys. Rev. Lett. **93**(17), 174102 (2004)
2. Agarwal, V., Balachandran, B.: Noise-assisted response steering for a rotor-stator system. J. Sound Vib. **523**, 116683 (2022)
3. Alofi, A., Acar, G., Balachandran, B.: Noise influenced response movement in coupled oscillator arrays with multistability. J. Sound Vib. **531**, 116951 (2022)
4. Bag, B.C., Petrosyan, K., Hu, C.-K.: Influence of noise on the synchronization of the stochastic kuramoto model. Physical Review E-Statistical, Nonlinear, and Soft Matter Physics **76**(5), 056210 (2007)
5. Balachandran, B., Breunung, T., Acar, G.D., Alofi, A., Yorke, J.A.: Dynamics of circular oscillator arrays subjected to noise. Nonlinear Dyn. **108**, 1–14 (2022)
6. Barone, A.: Physics and applications of the Josephson effect. Wiley, (1982)
7. Bello, L., Calvanese Strinati, M., Dalla Torre, E.G., Pe'er, A.: Persistent coherent beating in coupled parametric oscillators. Phys. Rev. Lett. **123**(8), 083901 (2019)
8. Breunung, T.: Asymptotic stability of quasi-periodic orbits. Proceedings of the Royal Society A **478**(2259), 20210787 (2022)
9. Breunung, T., Balachandran, B.: Computationally efficient simulations of stochastically perturbed nonlinear dynamical systems. J. Comput. Nonlinear Dyn. **17**(9), 091008 (2022)
10. Breunung, T., Balachandran, B.: Noise color influence on escape times in nonlinear oscillators-experimental and numerical results. Theor. Appl. Mech. Lett. **13**(2), 100420 (2023)
11. Breunung, T., Balachandran, B.: Nonlinear vibration attenuation via stochastic response modification. Journal of Computational and Nonlinear Dynamics, accepted, (2025)
12. Breunung, T., Kogelbauer, F., Haller, G.: The deterministic core of stochastically perturbed nonlinear mechanical systems. Proceedings of the Royal Society A, 478(2262), (2022)
13. Castanier, M.P., Pierre, C.: Modeling and analysis of mistuned bladed disk vibration: current status and emerging directions. J. Propul. Power **22**(2), 384–396 (2006)
14. Cilenti, L., Cameron, M., Balachandran, B.: Most probable escape paths in periodically driven nonlinear oscillators. Chaos: An Interdisciplinary Journal of Nonlinear Science, 32(8), (2022)

15. Dankowicz, H., Schilder, F.: Recipes for Continuation. SIAM, (2013)
16. Dörfler, F., Bullo, F.: Synchronization in complex networks of phase oscillators: A survey. Automatica **50**(6), 1539–1564 (2014)
17. Dykman, M., Krivoglaz, M.: Theory of fluctuational transitions between stable states of a nonlinear oscillator. Sov. Phys. JETP **50**(1), 30–37 (1979)
18. Fossen, T., Nijmeijer, H.: Parametric Resonance in Dynamical Systems. Springer Science & Business Media, (2011)
19. Freidlin, M.I., Wentzell, A.D.: Random Perturbations of Dynamical Systems. Springer, Berlin (2012)
20. Guckenheimer, J., Holmes, P.: Nonlinear oscillations, Dynamical systems, and Bifurcations of vector fields, volume 42. Springer Science & Business Media, (2013)
21. Hagedorn, P., Stadler, W.: Non-linear Oscillations. Clarendon Press, Oxford (1981)
22. Hoskoti, L., Gupta, S.S., Sucheendran, M.M.: Modeling of geometrical stiffening in a rotating blade—a review. J. Sound Vib. **548**, 117526 (2023)
23. Kiss, I.Z., Zhai, Y., Hudson, J.L.: Emerging coherence in a population of chemical oscillators. Science **296**(5573), 1676–1678 (2002)
24. Kovacic, I., Brennan, M.J.: The Duffing equation: nonlinear oscillators and their behaviour. John Wiley & Sons, (2011)
25. Kuramoto, Y.: Chemical Oscillations, Waves, and Turbulence. Springer, Berlin, Heidelberg (1984)
26. Lang, S.: Real and functional analysis, volume 142. Springer Science & Business Media, (2012)
27. Leissa, A., et al.: Vibrational aspects of rotating turbomachinery blades. Appl. Mech. Rev. **34**(5), 629–635 (1981)
28. MacKay, R., Aubry, S.: Proof of existence of breathers for time-reversible or hamiltonian networks of weakly coupled oscillators. Nonlinearity **7**(6), 1623 (1994)
29. Marandi, A., Wang, Z., Takata, K., Byer, R.L., Yamamoto, Y.: Network of time-multiplexed optical parametric oscillators as a coherent ising machine. Nat. Photonics **8**(12), 937–942 (2014)
30. Marin, J., Aubry, S.: Breathers in nonlinear lattices: numerical calculation from the anticontinuous limit. Nonlinearity **9**(6), 1501 (1996)
31. Martens, E.A., Thutupalli, S., Fourriere, A., Hallatschek, O.: Chimera states in mechanical oscillator networks. Proc. Natl. Acad. Sci. **110**(26), 10563–10567 (2013)
32. Martineau, S., Saffold, T., Chang, T.T., Ronellenfitsch, H.: Enhancing synchronization by optimal correlated noise. Phys. Rev. Lett. **128**(9), 098301 (2022)
33. Matkowsky, B.J., Schuss, Z.: The exit problem for randomly perturbed dynamical systems. SIAM J. Appl. Math. **33**(2), 365–382 (1977)
34. Matsumoto, K., Tsuda, I.: Noise-induced order. J. Stat. Phys. **31**, 87–106 (1983)
35. Motter, A.E., Myers, S.A., Anghel, M., Nishikawa, T.: Spontaneous synchrony in power-grid networks. Nat. Phys. **9**(3), 191–197 (2013)
36. Nair, N., Hu, K., Berrill, M., Wiesenfeld, K., Braiman, Y.: Using disorder to overcome disorder: A mechanism for frequency and phase synchronization of diode laser arrays. Phys. Rev. Lett. **127**, 173901 (2021)
37. Nayfeh, A.H., Balachandran, B.: Applied Nonlinear Dynamics: Analytical, Computational, and Experimental Methods. Wiley, New York (1995)
38. Nayfeh, A.H., Mook, D.T.: Nonlinear Oscillations. Wiley, New York (2008)
39. Neiman, A.B., Russell, D.F.: Synchronization of noise-induced bursts in noncoupled sensory neurons. Phys. Rev. Lett. **88**(13), 138103 (2002)
40. Pikovsky, A., Rosenblum, M., Kurths, J.: Synchronization: A Universal Concept in Nonlinear Sciences. Cambridge University Press, Cambridge Nonlinear Science Series (2001)
41. Sanders, J.A., Verhulst, F., Murdock, J.: Averaging Methods in Nonlinear Dynamical Systems, volume 59. Springer, (2007)
42. Strinati, M.C., Aharonovich, I., Ben-Ami, S., Dalla Torre, E.G., Bello, L., Pe'er, A.: Coherent dynamics in frustrated coupled parametric oscillators. New J. Phys. **22**(8), 085005 (2020)
43. Strogatz, S.H.: From kuramoto to crawford: exploring the onset of synchronization in populations of coupled oscillators. Physica D **143**(1–4), 1–20 (2000)
44. Strogatz, S.H.: Exploring complex networks. Nature **410**(6825), 268–276 (2001)
45. Vanag, V.K., Yang, L., Dolnik, M., Zhabotinsky, A.M., Epstein, I.R.: Oscillatory cluster patterns in a homogeneous chemical system with global feedback. Nature **406**(6794), 389–391 (2000)
46. Verhulst, F.: Methods and Applications of Singular Perturbations: Boundary Layers and Multiple Timescale Dynamics, volume 50. Springer Science & Business Media, (2006)
47. Watts, D.J., Strogatz, S.H.: Collective dynamics of 'small-world' networks. Nature **393**(6684), 440–442 (1998)
48. Wiesenfeld, K., Colet, P., Strogatz, S.H.: Synchronization transitions in a disordered josephson series array. Phys. Rev. Lett. **76**(3), 404 (1996)
49. Womelsdorf, T., Schoffelen, J.-M., Oostenveld, R., Singer, W., Desimone, R., Engel, A.K., Fries, P.: Modulation of neuronal interactions through neuronal synchronization. Science **316**(5831), 1609–1612 (2007)
50. Yakubovich, V., Starzhinskii, V.: Linear differential equations with periodic coefficients. Wiley, New York, (1975 - 1975)
51. Zhou, C., Kurths, J., Kiss, I.Z., Hudson, J.L.: Noise-enhanced phase synchronization of chaotic oscillators. Phys. Rev. Lett. **89**(1), 014101 (2002)